Iron(III) complexing ability of new ligands based on natural γ-pyrone maltol

Fusi, S.; Frosini, M.; Biagi, M.; Zor, K.; Rindzevicius, T.; Baratto, M. C.; De Vico, L.; Corsini, M.

Published in:
Polyhedron

Link to article, DOI:
10.1016/j.poly.2020.114650

Publication date:
2020

Document Version
Peer reviewed version

Iron(III) complexing ability of new ligands based on natural γ-pyrone maltol

S. Fusi,[a] M. Frosini,[b] M. Biagi,[c] K. Zór,[d] T. Rindzevicius,[d] M. C. Baratto,[a] L. De Vico[a], M. Corsini*[a]

[a] Department of Biotechnology, Chemistry and Pharmacy, University of Siena, Via A. Moro 2, 53100 Siena, Italy

[b] Department of Life Sciences, University of Siena, via A. Moro 2, 53100 Siena, Italy

[c] Department of Physical Sciences, Earth and Environment, University of Siena, Strada Laterina 8, 53100 Siena, Italy

[d] The Danish National Research Foundation and Villum Foundation's Center for Intelligent Drug Delivery and Sensing Using Microcontainers and Nanomechanics (IDUN), Department of Health Technology, Technical University of Denmark, Ørsteds Plads, Building 345C 2800, Kgs. Lyngby, Denmark

*Corresponding author: maddalena.corsini@unisi.it (Maddalena Corsini)

Abstract

Two new hydrophilic maltol derivatives were prepared with the aim of designing a chelator able to solubilize Fe(III) by complexation in physiologic condition. Sodium 2-((2-methyl-4-oxo-4H-pyran-3-yl)oxy)malonate (**3**) and lithium 2-((3-hydroxy-4-oxo-4H-pyran-2-yl)methyl)malonate (**7**) were prepared and characterized by ^{1}H- and ^{13}C-NMR and their antioxidant properties were evaluated. The results indicate that the hydroxyl radical scavengers activity measured by deoxyribose degradation method, was comparable to maltol (Malt) itself (IC_{50} 5.58±0.76, 2.14±0.46 and 2.44±0.1 of (**7**), (**3**) and Malt respectively). However, the antiradical activity measured by DPPH method, follows the order (**7**) > (**3**) > Malt (IC_{50} 3.15 ± 0.40; 4.96 ± 0.29; > 7 mM, respectively). Additionally, their Fe(III) chelation ability was investigated in aqueous solution by means of electrochemical, various spectroscopic (UV-Vis, IR, EPR and Raman) and computational methods. The spectroscopic and theoretical elucidation indicates the main bidentate nature of ligand (**3**), coordinated *via* deprotonated carboxylic oxygen atoms of malonate moiety, while ligand (**7**) may coordinate also through phenolic and carbonyl oxygen atoms of maltol unity.

Moreover, cyclic voltammetry studies suggest that the reduction of ferric complexes to more labile Fe(II) species proceeds in dissociation of the starting complexes. The obtained results point out the potential of these ligands in oral iron supplementation therapy.

Keywords

Hydroxypyrones, iron, redox chemistry, maltol derivatives, antioxidant, antiradicalic

Graphical abstract

Two new Fe(III) ligands based on natural γ−pyrone maltol were synthetized with the aim to obtain compounds with potential use as an oral therapy for iron deficiency.

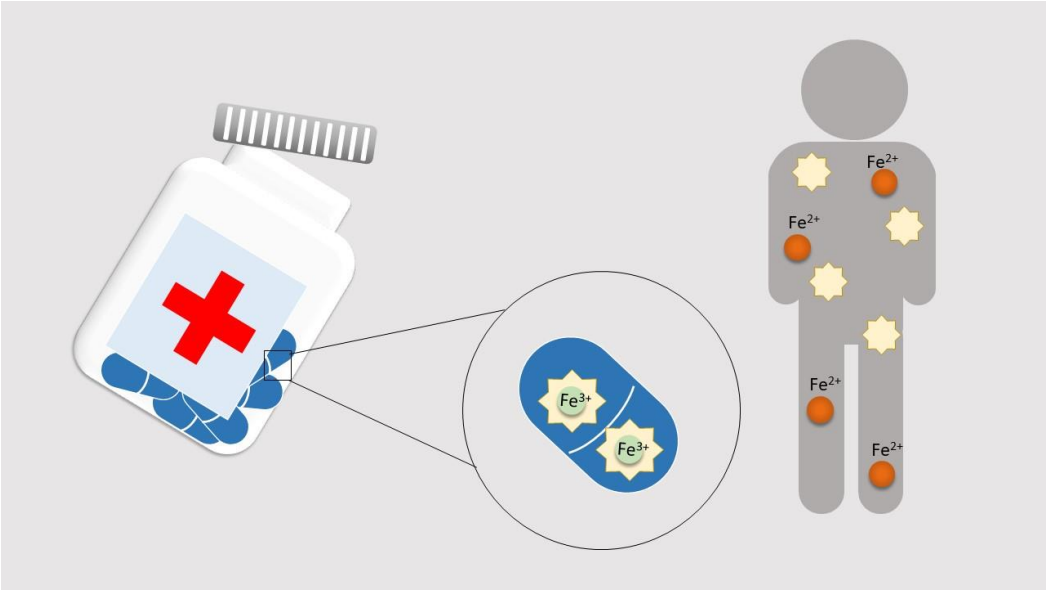

Abbreviation

ID, iron deficiency; $TBAPF_6$, tetrabutylammonium hexafluorophosphate; NHE, normal hydrogen electrode, EDTA, ethylendiaminetetracetic acid; DPPH, 1,1-diphenyl-2-picryl-hydrazyl; Malt, maltol; EPR, electron paramagnetic resonance.

1. Introduction

Iron deficiency (ID) is a common hematological problem affecting most patients with inflammatory bowel disease, pregnant women, as well as it is a frequent complication in patients with solid tumors, especially if treated with chemotherapeutic agents. [1,2]

Traditionally, oral iron supplementation is frequently used to treat ID anemia, since it is safe, easy to administer and has a low cost. The most widely used formulations contain Fe(II) form (ferrous

sulfate, ferrous gluconate, and ferrous fumarate), that can be directly absorbed by enterocytes in the small and large intestine. [3] However, it has been reported that at the gastrointestinal mucosa level, Fe(II) preparations are, likely, involved in oxidative damage to cell membranes through the formation of free radicals. [4,5] Gastrointestinal adverse effects associated with oral Fe(II) treatment are often reported, including nausea, flatulence, abdominal pain and constipation. [6] Therefore, it is highly desired to design new iron supplements with no or few side effects. Use of Fe(III) preparations should avoid these widespread problems. In fact, they provide better stability for traditional ferrous compounds as they could more easily penetrate the intestinal mucosa. On the other hand, ferric preparations are rapidly converted to poorly absorbed iron hydroxide species when passing from the acidic environment of the stomach to the more neutral pH of the duodenum, consequently their bioavailability is lower than that of conventional ferrous salts. [3,7] Inhibition of this hydroxide species formation and a more rapid transit through the mucus layer would facilitate ferric iron absorption. To pursue this goal, the idea is to use a Fe(III) chelator that forming stable ferric complex at neutral pH, prevents formation of iron hydroxide polymers and makes the metal more available in the intestinal tract.

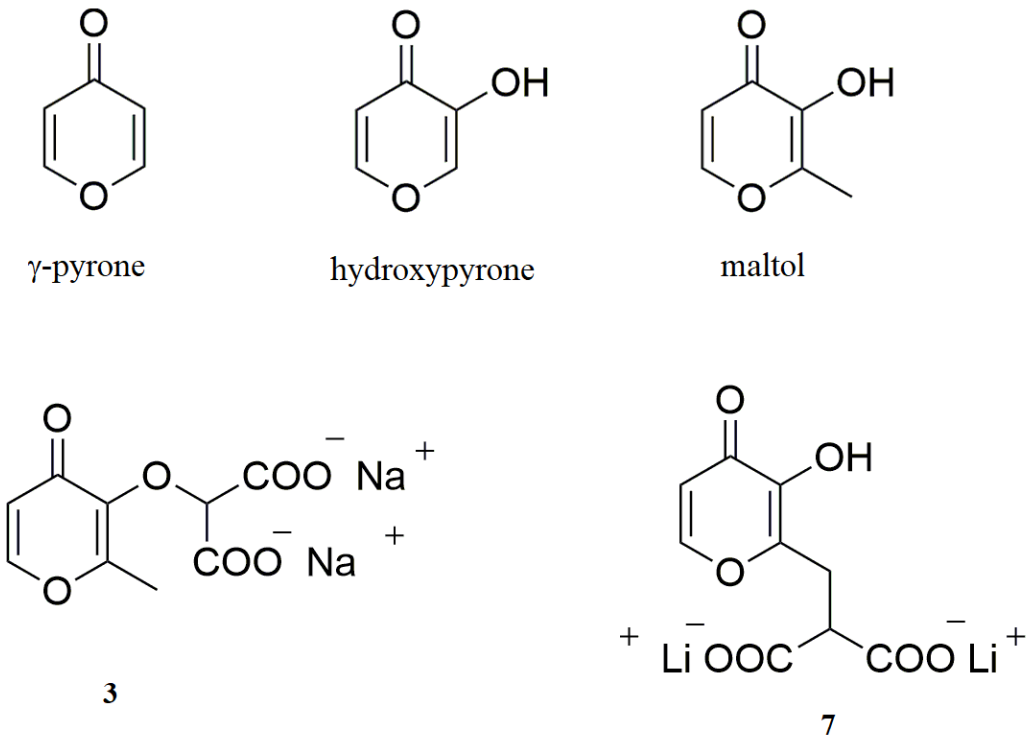

Scheme 1

γ-Pyrone (Scheme 1) constitutes the core of an interesting class of natural compounds such as flavones and 3-hydroxy-4-pyrones (also referred to as hydroxypyrones hereafter). Hydroxypyrones are O-heterocyclic chelators containing two vicinal oxygen atoms belonging to carbonyl and hydroxyl groups, which confer high affinity towards M^{III} metal ions. Maltol (3-hydroxy-2-methyl-4-pyrones), presented in Scheme 1 above, is readily available from natural sources and is widely used in food and cosmetics additives, as well as in many derivatives design for medical applications [5], [8], [9], [10]. The advantages of using maltol for clinical purposes are its strong metal binding affinity (good iron chelator), high bioavailability and a low toxicity profile [11],[12], [13],[14]. Furthermore, maltol prevents the iron-catalyzed formation of free radicals and free radical cascades by binding this metal ion and render it redox inactive. [11]

Nowadays, the European Medicines Agency (EMA) and the US Food and Drug Administration (FDA) approve ferric maltol (Feraccru/Accrufer; Shield Therapeutics, Inc.) as an alternative oral treatment for ID anemia in adults [15], [16], [17]. After oral ingestion of ferric maltol, Fe(III) reaches the intestinal mucosa in complex form, which is believed to allow more efficient uptake of iron into enterocytes compared with ferrous iron salts [18],[19].

There is a growing research area focused on the improvement of iron formulations for oral supplementation, aimed to obtain novel products that may adequately fulfil biological requirements and patient's needs. In this work, we report the synthesis and characterization of new, water-soluble iron chelators containing a γ-pyrone core. The basic concept is to introduce carboxylic functional groups into the biologically active compound, so as to obtain a higher aqueous solubility, while also increasing the number of coordinating oxygen atoms, all this without changing the properties connected to the γ-pyrone core structure. Indeed, most oral drugs are absorbed in the small intestine (pH 6.0-7.8) where acidic compounds are, mainly, anions. Therefore, they are associated with a poor permeability because barely cross negatively charged lipid membranes. [20] In this way, suggested compounds should be able to deliver and release iron to the intestine mucosa, but not be absorbed by it, and thus easily discarded.

Here we present the physical-chemical characterization (sections 3.1 and 3.2) and the iron(III) complexing ability (evaluated by electrochemical and spectroscopic methods such as IR, UV-vis, Raman and Electron Paramagnetic Resonance, section 3.3) of the new γ-pyrone compounds. Since we were not able to obtain X-ray crystallographic data of the ferric complexes, we studied them computationally, and thus reinforce the suggested chelating modes of ligands (**3**) and (**7**) (section 3.3.3). Finally, we present an analysis of antioxidant properties of the new compounds (section 3.3.6) with respect to maltol.

2. Experimental

2.1 Syntheses

*2.1.1. Diethyl 2-((2-methyl-4-oxo-4H-pyran-3-yl)oxy)malonate (**2**)*

To a stirred solution of maltol (**1**) (10 mmol) and K_2CO_3 (20 mmol) in dry CH_2Cl_2 at room temperature diethylbromomalonate (15 mmol) was added and the mixture was refluxed overnight. The dark orange solution was washed with H_2O, dried over Na_2SO_4, filtered and solvent removed under reduced pressure. Purification of residue by flash chromatography with petroleum ether-ethyl acetate (8:2) as eluent gave pure compound (**2**) as a yellow oil (yield 62%). ^{1}H-NMR (400MHz, $CDCl_3$): δ (ppm) 1.24 (t, 6H, J = 7.2 Hz, $OCH_2\underline{CH_3}$), 2.39 (s, 3H, 2-CH_3), 4.18-4.28 (m, 4H, $O\underline{CH_2}CH_3$), 5.67 (s, 1H, H2), 6.26 (d,1H, J = 5.6 Hz, H5), 7.58 (d,1H, J = 5.6 Hz, H6). ^{13}C-NMR (100MHz, $CDCl_3$): δ (ppm) 13.91, 15.01, 61.98, 77.27, 116.93, 142.69, 153.62, 159.56, 165.76, 173.75. ESI-MS: m/z 307(M+Na).

*2.1.2. Sodium 2-((2-methyl-4-oxo-4H-pyran-3-yl)oxy)malonate (**3**)*

Diethyl 2-((2-methyl-4-oxo-4H-pyran-3-yl)oxy)malonate was stirred at room temperature with an aqueous solution of NaOH (1:2) overnight to give the final hydrolyzed compound. The aqueous solution was evaporated under reduced pressure and the crude was washed with CH_2Cl_2 and MeOH to obtain the compound (**3**) as a white solid (yield 80%). ^{1}H-NMR (400MHz, D_2O): δ (ppm) 2.40 (s, 3H, 2-CH_3), 4.89 (s, 1H, H2), 6.42 (d,1H, J = 5.6 Hz, H5), 7.92 (d, 1H, J = 5.6 Hz, H6). ^{13}C-NMR (100MHz, D_2O): δ (ppm) 14.98, 114.95, 116.58, 142.80, 156.02, 163.47, 174.30, 176.76. ESI-MS: m/z 227(M+H), 249(M+Na).

*2.1.3. Diethyl 2-((3-methoxy-4-oxo-4H-pyran-2-yl)methyl)malonate (**5a**) Dimethyl 2-((3-methoxy-4-oxo-4H-pyran-2-yl)methyl)malonate (**5b**)*

To a mixture of diethylmalonate or dimethylmalonate (5 mmol) and NaH 60% (5 mmol) in benzene at room temperature was added dropwise a benzene solution of 2-(bromomethyl)-3-methoxy-4H-pyran-4-one (**4**) (5 mmol) [21]. After 2h of stirring the solvent was removed under reduced pressure. The resulting crude was washed with H_2O and extracted with CH_2Cl_2 (3 x 15 mL). The combined organic layers were dried over Na_2SO_4, filtered and the solvent was removed under reduced pressure. The residue was purified by column chromatography on silica gel (petroleum ether-ethyl acetate 3:2) to give diethyl 2-((3-methoxy-4-oxo-4H-pyran-2-yl)methyl) malonate (**5a**) as pale yellow oil (yield 50%) ^{1}H-NMR (400MHz,$CDCl_3$): δ (ppm) 1.18 (t, 6H, J = 7.2 Hz, OCH_2CH_3), 3.21 (d, 2H, J = 7.8 Hz, CH_2), 3.72 (t, 1H, J = 7.8 Hz, CH), 3.82 (s, 3H, OCH_3), 4.09-4.19 (m, 4H, OCH_2CH_3), 6.28 (d,1H, J = 5.4 Hz, H5), 7.56 (d,1H, J = 5.4 Hz, H6). ^{13}C-NMR (100MHz, $CDCl_3$): δ (ppm) 13.78, 27.38, 48.75, 59.87, 61.71, 117.17, 145.90, 153.29, 157.44, 167.83, 164.68. ESI-MS: m/z 299(M+H), 321(M+Na), or dimethyl 2-((3-methoxy-4-oxo-4H-pyran-2-yl)methyl) malonate (**5b**) as yellow oil (Yield 48%) ^{1}H-NMR (400MHz,$CDCl_3$): δ (ppm) 3.28 (d, 2H, J = 7.6 Hz, CH_2), 3.74(s, 6H, $COOCH_3$), 3.81 (t, 1H, J = 7.6 Hz, CH), 3.88(s, 3H, OCH_3), 6.33 (d,1H, J = 5.6 Hz, H5), 7.59(d,1H, J = 5.6 Hz, H6). ESI-MS: m/z 271(M+H).

*2.1.4. Diethyl 2-((3-hydroxy-4-oxo-4H-pyran-2-yl)methyl)malonate (**6a**) Dimethyl 2-((3-hydroxy-4-oxo-4H-pyran-2-yl)methyl)malonate (**6b**)*

To a dry CH_2Cl_2 solution of diethyl 2-((3-methoxy-4-oxo-4H-pyran-2-yl)methyl)malonate (**5a**) or dimethyl 2-((3-methoxy-4-oxo-4H-pyran-2-yl)methyl)malonate (**5b**) (2 mmol) a BBr_3 1 N solution in CH_2Cl_2 (10 mmol) was added at 0 °C. The mixture was stirred at room temperature for 6 h and washed with $NaHCO_3$ saturated solution. The organic layer was dried over Na_2SO_4, filtered, the solvent was removed under reduced pressure to give diethyl 2-((3-hydroxy-4-oxo-4H-pyran-2-yl)methyl)malonate (**6a**) as white solid (yield 95%). m.p. 75-76 °C ^{1}H-NMR (400MHz, $CDCl_3$): δ (ppm) 1.19 (t, 6H, J = 7.2 Hz, $OCH_2\underline{CH_3}$), 3.28 (d, 2H, J = 8.0 Hz, CH_2), 3.80 (t, 1H, J

= 8.0 Hz, CH), 4.08-4.20 (m, 4H, O$\underline{CH_2}CH_3$), 6.38 (d,1H, J = 5.4 Hz, H5), 7.67 (d,1H, J = 5.4 Hz, H6). ^{13}C-NMR (100MHz,$CDCl_3$): δ (ppm) 13.76, 27.49, 48.63, 61.67, 113.02, 143.49, 147.80, 154.26, 167.90, 172.93. ESI-MS: m/z 285(M+H), 307 (M+Na), or dimethyl 2-((3-hydroxy-4-oxo-4H-pyran-2-yl)methyl)malonate (**6b**) as white solid (yield 90%). m.p.120-122°C ^{1}H-NMR (400MHz,$CDCl_3$): δ (ppm) 3.32 (d, 2H, J = 7.6 Hz, CH_2), 3.74(s, 6H, $COOCH_3$), 3.86 (t, 1H, J = 7.6 Hz, CH), 6.40 (d,1H, J = 5.2 Hz, H5), 7.69 (d,1H, J = 5.2 Hz, H6). ^{13}C-NMR (100MHz,$CDCl_3$): δ (ppm) 27.77, 48.44, 52.92, 113.34, 143.73, 147.90, 154.58, 168.47, 173.22. ESI-MS: m/z 257(M+H).

*2.1.5. Lithium 2-((3-hydroxy-4-oxo-4H-pyran-2-yl)methyl)malonate (**7**)*

Diethyl 2-((3-hydroxy-4-oxo-4H-pyran-2-yl)methyl)malonate (**6a**) or dimethyl 2-((3-hydroxy-4-oxo-4H-pyran-2-yl)methyl)malonate (**6b**) was hydrolyzed to a final compound (**7**) and stirred at room temperature with an aqueous solution of LiOH (1:4) overnight to give final hydrolyzed compound (**7**). The aqueous solution was evaporated under reduced pressure. The resulting crude was washed with CH_2Cl_2 and MeOH to obtain the compound as a white solid (yield 80%). ^{1}H-NMR (400MHz,D_2O): δ (ppm) 3.06 (d, 2H, J = 7.6 Hz, CH_2), 3.37 (t, 1H, J = 7.6 Hz, CH), 6.29 (d,1H, J = 5.2 Hz, H5), 7.74 (d,1H J = 5.2 Hz, H6). ^{13}C-NMR (100MHz, D_2O): δ (ppm) 29.29, 38.26, 151.55, 153.19, 153.47, 154.82, 178.74, 180.80. ESI-MS: m/z 227(M+H).

2.2. X-Ray crystallography

Single crystal X-ray diffraction experimental conditions and refinement are detailed in Supporting Information (Table S1 and S2). The supplementary crystallographic information for this paper can be found free of charge from the Cambridge Crystallographic Data Centre via www.ccdc.cam.ac.uk/data_request/cif under CCDC 1891539. All measurements were performed

at the “C.R.I.S.T.”, University Service Centre for Structural Crystallography, University of Florence.

2.3 Materials and spectroscopic measurements

All chemicals were purchased from commercial suppliers and used without further purification. The organic reagents used, as well as the solvents, were pure commercial products from Sigma-Aldrich (Milan, Italy).

Melting point was measured with a Kofler apparatus and was uncorrected. The ^{1}H and ^{13}C NMR spectra were recorded at 400.13 MHz and 100.13 MHz on a Bruker Advance DPX400 instrument. Chemical shifts were reported relative to tetramethylsilane at 0.00 ppm. ESI-MS spectra were recorded with a LCQ-DECA Thermo Finnigan instrument. TLC was performed on precoated 4 × 6.7 silica gel 60 F254 plates silica gel on aluminum with detection by UV light. Column chromatography was carried out on Silica gel (Merck Inc., Milan, Italy, 0.040 - 0.063 mm). The FTIR spectra were recorded using Spectrum BX (Perkin-Elmer, USA) with a resolution of 4 cm^{-1} from 400 to 4000 cm^{-1}. The samples used for IR spectroscopy were prepared adding appropriate amount of ligand (0.003 mol) to 10 mL of an aqueous solution of $Fe(NO_3)_3$ x $9H_2O$ (0.001 mol). After that, the acidity of reaction medium was brought to pH 2.0. The reaction mixture was stirred for 15 minutes, and then evaporated in a rotary evaporator. The samples were dried under vacuum at room temperature. Finally, KBr disks for IR spectroscopy measures were prepared. UV-Vis spectra of compounds were recorded in a Lambda 900 Spectophotometer (Perkin Elmer, U.S.A.) at room temperature.

All Raman scattering measurements were performed using a Thermo Fisher Scientific DXR Raman microscope (Thermo Fisher Scientific, Inc., Waltham, MA, USA). The microscope

was coupled to a single-grating spectrograph, the spectral resolution is about 5 cm-1 fwhm with a ±2 wavenumber accuracy. The Raman signal collection time was 30 s, the signal was averaged over 3 exposures using a 50 µm slit, a 10x objective lens, 24 mW laser power, and a 0.8 µm in diameter laser spot. Liquids were pipetted into a 0.5 mL stainless steel cavity and the laser focus was positioned in the middle of the liquid volume. The recorded Raman scattering signal was background corrected and spectra were off-shifted for clarity. For measurements, ligands (**3** and **7**) and maltol (5 mg) were dissolved in 50 µL ultrapure water obtained from a Milli-Q water purification system (Millipore Corporation, Billerica, MA, USA). The $Fe(NO_3)_3$ was dissolved in 10 mM HCl having the final concentration of 100 mg/mL . The mixture of ligand in water (30 µL), $Fe(NO_3)_3$ in HCl (30 µL) and the 40µL of the relevant buffer solution (phosphate pH 7.2 or acetate pH 4.4 buffer) were prepared and measurements were carried out in stainless steel holder using 100 µL of sample at laser intensity, type of laser.

130K EPR spectra were recorded at X-band (9.6GHz) with a Bruker Elexsys E500 Series, (Bruker BioSpin GmbH, Rheinstetten, Germany) using the Bruker ER4122SHQE cavity and an Oxford helium continuous flow cryostat (ESR900). The concentration of the solutions is 0.001 M of $Fe(NO_3)_3$ and 0.003M of ligands . The sample was placed in a quartz-suprasil capillary with a diameter of 3mm and it was frozen out of the spectrometer into liquid nitrogen.

2.4 Electrochemical and spectroelectrochemical measurements

Voltammetric measurements were performed in 0.1 M KNO_3 solution using a three-electrode cell equipped with a glassy carbon working, a platinum auxiliary and Ag/AgCl reference electrodes. All the solutions were degassed with nitrogen before experiment. Sweep rates were varied between 20 and 500 mV/s, to check the reversibility of the redox couple. A BAS100W electrochemical analyzer (Bioanalytical Systems, Inc., U.S.A.) was used as the polarizing unit. Spectroelectrochemical experiments were carried out on Lambda 2 (Perkin Elmer, U.S.A.).

UV/Vis spectrophotometer for spectra data acquisition while the electrode potential was controlled by BAS100W electrochemical analyzer. Cyclic voltammograms were recorded at 1 mV/s scan rate between 0 to -0.90 V. UV/Vis spectra were recorded between 220 and 800 nm at the scan rate of 960 nm/min. The cell used was a SEC-C cell (Thin Layer Quartz Glass Spectroelectrochemical Cell) equipped with a Pt gauze working electrode (80 mesh), a Pt counter electrode and Ag/AgCl (KCl 3M) as reference electrode. Nitrogen-saturated solutions of the compounds were used with phosphate or acetate buffer (0.1 M) as supporting electrolyte.

2.5 Deoxyribose degradation assay

The scavenging activity of compounds (maltol and ligands) was determined by the deoxyribose degradation assay, which uses H_2O_2 and Fe(III)–EDTA complex to generate hydroxyl radicals using to the established protocol with few modifications.[22] Briefly, each sample contained 20 mM KH_2PO_4/K_2HPO_4 buffer pH 7.4, tested compounds (generally in the range 1-10 mM), 2.8 mM deoxyribose, 0.1 mM $FeCl_3$, 0.1 mM EDTA, 0.2 mM H_2O_2 and 0.1 mM ascorbic acid (the latter used to start the reaction) in a final volume of 1 ml. All the solutions were prepared immediately before use.

Samples were incubated a 37 °C for 1 h, added with 1 mL of 2.8% (w/v) trichloroacetic acid and 1 mL of 1% (w/v), thiobarbituric acid in 50 mM NaOH, and then heated at 100 °C (15 min in a boiling water bath). Absorbance of the resulting solutions was measured at 532 nm by using UV-vis spectrophometer Lambda 2.

For all concentrations of the tested compounds, controls with deoxyribose-free reaction mixture were also performed. Maltol, and ligands (**3**) and (**7**) as well as deoxyribose, released TBA-reactive products when attacked by HO•. Thus, the absorbance values obtained for these samples were subtracted from those of complete assays plus the ligands [23].

Results are reports as mean±s.e.m. from at least three independent experiments. IC_{50} (concentration of the compound which caused 50% of the inhibition of the formation of the pink chromogen) were calculated by fitting log [inhibitor] *vs* normalized response (variable slope) (GraphPad Software Inc.) [24].

2.6 DPPH assay

The antiradicalic capacity of compounds was evaluated using the DPPH reagent according to the method published by Biagi et al. [25]. Briefly, 0.1 mL of water solutions of the different samples (140 to 1 mM) were added to 1.9 ml of freshly prepared methanolic DPPH solution (1 x 10^{-4} M) and stirred. The decolorizing process at the beginning of reaction and after 20 min was recorded at 517 nm and compared with a blank control. Antiradicalic activity was calculated according to the following formula:

Antiradicalic activity % = [(control absorbance-sample absorbance) / (control absorbance)] x 100.

IC_{50} (mean ± e.s.m, x10^{-3} M) for each compound was calculated as previously described.

2.7 Computational Methods

Several models of possible complexes between Fe(III) and compounds (**3**) and (**7**) were tested with computational means, as reported in Table 1. The geometry of each model was optimized at the Density Function Theory (DFT) level of theory, [26] employing the 6-31G* basis set [27] and the B3LYP functional. [28] Although, a number of explicit water molecules were included in the models, to complete the complexation of the iron ion, the optimized geometries were further refined applying the Polarizable Continuum Model (PCM) [29] method for implicit solvent effects, using water as solvent. All models contained Fe(III) ion, was considered in a high-spin state (5 electrons with the same spin), thus unrestricted Hartree-Fock was employed as reference wave function. Both compound (**3**) and (**7**) were considered as closed-shell systems; compound (**3**) was

considered as carrying a -2 charge, while a -3 charge was assigned to compound (**7**), that is when also its hydroxyl group is deprotonated. The overall charge of each model is reported in Table 1. The Cartesian coordinates of the optimized models, along with their corresponding absolute energies, are given as supporting information. All calculations were performed using the OpenMolcas software package, version 18.09 [30].

Table 1
Fe(III) complexes computational models, with different numbers of ligand and explicit water molecules.

Model	Ligand	Number of Ligand Molecules	Number of Explicit Water Molecules	Overall Charge
Model 1	Compound (3)	1	4	+1
Model 2	Compound (3)	2	2	-1
Model 3	Compound (7)	1	4	0
Model 4	Compound (7)	1	4	0
Model 5	Compound (7)	2	2	-3
Model 6	Compound (7)	2	2	-3
Model 7	Compound (7)	2	2	-3

3. Results and discussion

3.1 Synthesis and characterization

The compounds (**2**) and (**3**) were obtained with a nucleophilic substitution of the maltol anion over diethylbromomalonate and followed by basic hydrolysis, as shown in Scheme 2.

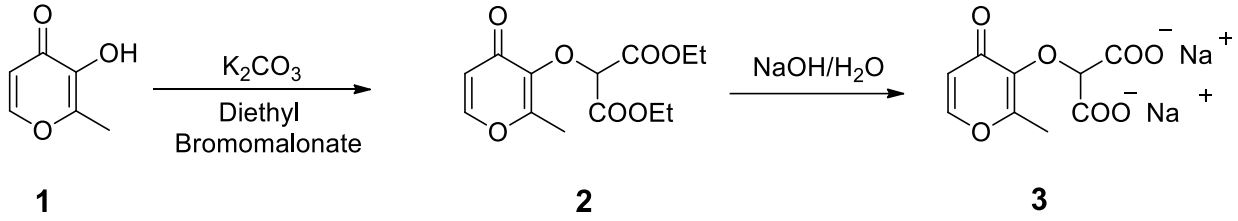

1 **2** **3**

Scheme 2. Synthetic route of hydroxypyrone derivatives (**2**) and (**3**)

For the synthesis of the other studied ligand, compound (**7**) we have first protected the hydroxyl group of maltol, brominated the methyl group which underwent the nucleophilic attack of the malonate anion. The deprotection of the OH group and subsequent hydrolysis is necessary (Scheme 3).

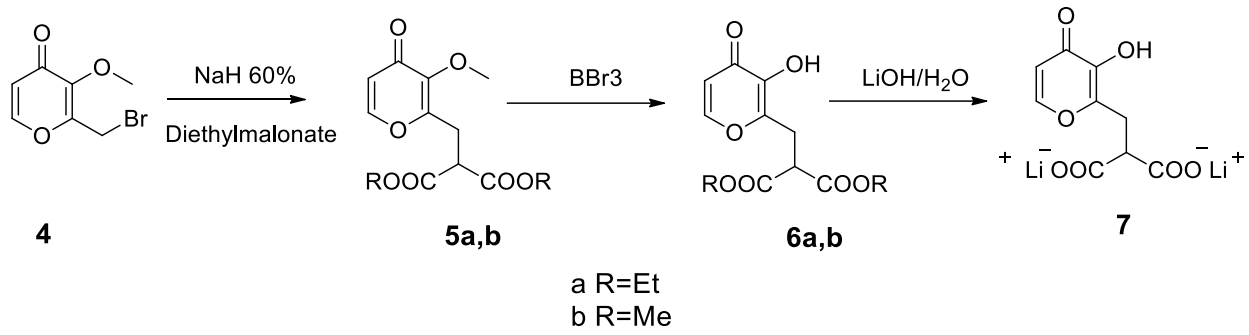

Scheme 3. Synthesis of the hydroxypyrone derivatives (**4**-**7**)

After slow evaporation of methanolic solution of (**6b**), white single-crystals suitable for a single-crystal X-ray diffraction study were obtained. It crystallized in the monoclinic space group P2(1)/n with eight molecules in the unit cell. Crystallographic data, bond lengths and bond angles are summarized in Table S1 and S2.

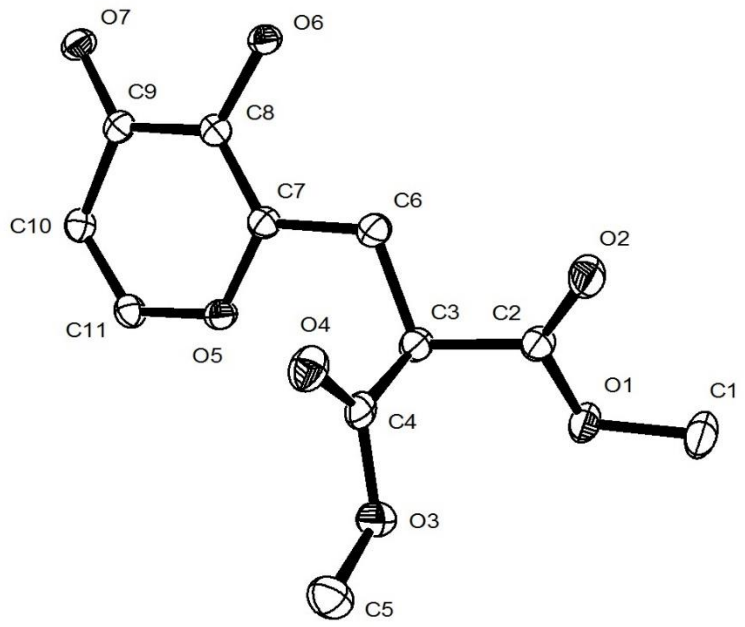

Fig. 1. An ORTEP view of the crystal structure of (**6b)** (thermal ellipsoids with 50 % probability). CCDC 1891539

The hydroxopyrone moiety is stabilized by one intramolecular H-bond involving the OH group as donor and the carbonyl oxygen as acceptor [O6 – H6 ⋯ O7 (2.36(5) Å, 111.5°)]. Existence of a five-membered quasi-ring with an intermolecular H-bond is recurrent in neutral hydroxypyrone. Furthermore, O6 and O7 oxygen atoms are involved in an intermolecular H-bond (Figure S1).

3.2 Physical-chemical characterization of the ligands

The compounds (**2**), (**6a-b**) were reaction intermediates with poor water solubility, therefore they were not further investigated. The ligands (**3**) and (**7**) were characterized in terms of their dissociation constants, UV-visible and solution stability. In addition, their pK_as were estimated by

potentiometric and/or spectrophotometric titration (25 °C, 0.1 M KNO_3). The spectroscopic titration of (**7**) was possible following the shift of the band attributable to the dissociation of OH group of hydroxypyrone [31]. Table 2 summarizes the stepwise dissociation constant (pK_i) calculated for the new molecules as well as for maltol, taken as reference compound [23]. The dissociation constants pK_1 and pK_2, of the first and second proton, ranging from 3.1 to 5.1. Those values were comparable with malonic acid dissociation constants [32]. In agreement with maltol, the pK_3 for the acid dissociation of the hydroxyl group in (**7**) was roughly 8.5.

Table 2. Dissociation constants (p*Ki,*) and partition coefficients of investigated ligands (**3**), (**7**) and maltol.

	$(\mathbf{3})^{2-}$	$(\mathbf{7})^{2-}$	**Malt**
Molecular weight	226.14	226.14	126.11
pK_1	3.16[a]	3.91[a]	-
pK_2	3.99[a]	5.06[a]	-
pK_3	-	9.17[b]	8.54[c]
Log P	-7.05[d]	-7.08[d]	-0.04[c] ; 0.85[d]
HBD	2	3	1
HBA	7	7	3

[a] Potentiometric data. [b] Determined by spectrophotometric titration: [**7**]=6.3x10^{-5} M. [c] From ref [23]. [d] Calculated logP value used ChemAxon algoritm [33].

The species distribution diagram of (**7**) was obtained by using the simulation program HySS [34] (Figure 2).

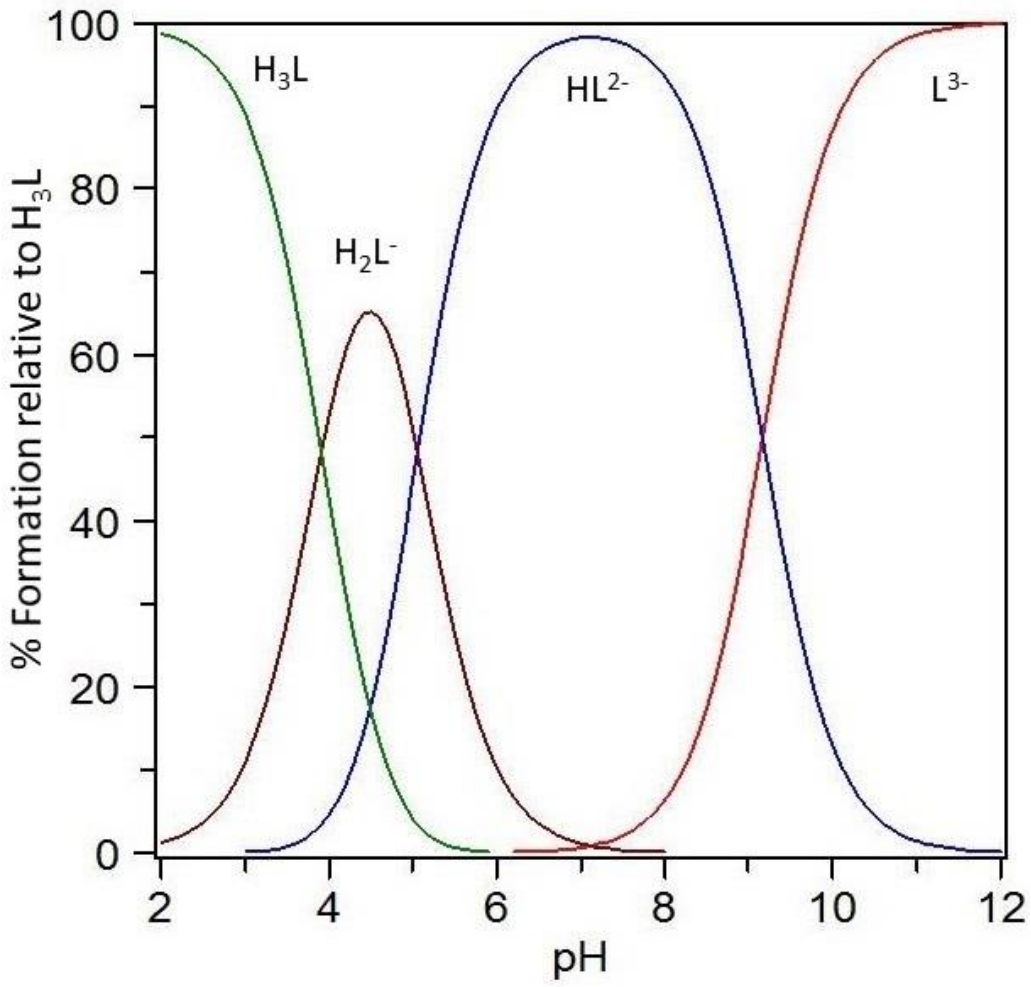

Fig. 2. Species distribution plot calculated for the ligand (**7**).

Lipophilicity of molecules was assessed by calculation of partition coefficients (Log P). A lower water solubility of maltol compared to (**3**) and (**7**) was supported by higher Log P values (Table 2). In general, malonate salts **(3**) and (**7**) were highly water soluble in accordance with the fact of a greater degree of H-bond formation.

Traditionally, therapeutics are small molecules that fall within the Lipinski's rule of 5, Ro5. The rule predicts that poor absorption or permeation of biological membrane is more likely when a drug has more than 5 H-bond donors (HBD, expressed as sum of OH and NH groups), 10 H-

bond acceptors (HBA, expressed as sum of O and N atoms), molecular size is greater than 500 g/mol and Log P greater than 5 [345]. As reported in Table 2, compounds (**3**) and (**7**) fulfill Ro5, therefore these ligands can be envisioned as possible orally delivered drugs.

Another important feature is solution stability of molecule in physiologic environment. This is important in drug development because the compounds should not undergo any reaction with oxygen, water or other excipients presents in solution in the gastrointestinal tract, which could compromise their structure and activity.

The solution stability of ligands (**3**) and (**7**) in phosphate buffered solution (maintained at 37°C for 72 hours) was assessed by recording the UV-vis spectra every 24 hours. Upon 72 hours of incubation there were no changes in the UV-vis spectra in either ligands (**3**) and (**7**) (Fig. 3).

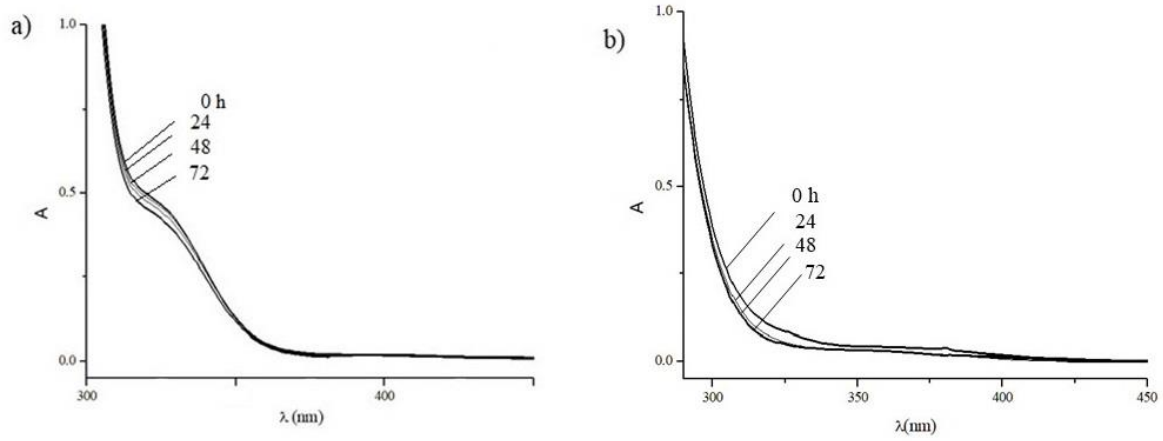

Fig 3**.** Time-dependent stability of: (a) (**7**) 8.2 x 10^{-4} M, and (b) (**3**) 2.2 x 10^{-4} M monitored by UV–vis absorption spectra over a period of 72 hours. Compounds were dissolved in PBS pH 7.4 and incubated at 37 °C for 24, 48, 72 h.

3.3 Iron complexation studies

Several experiments were performed in order to obtain a single crystal of ferric complexes; unfortunately, instead of single crystal, a glass-like structure was obtained in all cases. Therefore, further characterization was carried out in solution.

3.3.1 UV-Vis spectroscopy

Because its chemical structure, ligand **3** could coordinates Fe(III) only through oxygen atoms of malonate moiety. As far as the formation of ferricarboxylate complexes is concerned, literature reports that, at pH acid malonic acid forms complexes with Fe(III). [36] Consequently, we are expecting that Fe(III)/(**3**) solution had a spectral profile similar to other ferric complexes of β-diketones. [37], [38], [39] In fact, at pH 4.5 Fe(III)/(**3**) solution showed the single symmetric peak of ligand at 263 nm and a shoulder band around 320 nm. Increasing pH, the absorbance of this lower wavelength peak increased till to pH > 8.5 when precipitation occurred.

Differently, ligand (**7**) could coordinate metal in different ways, precisely: i) *via* oxygen atoms of malonate moiety, in the same fashion of (**3**), ii) *via* the phenol and keto oxygen atoms of hydroxypyrone ring, and iii) *via* both modes at the same time. As Figure 4 shows, addition of Fe(III) to an aqueous solution of (**7**) determined the appearance of a broad band at 520 nm (pH 0.5, grey line). Increasing pH, two more intense absorptions appeared at wavelength of 490 and 400 nm. However, the intensity of such bands disappeared at pH > 5.5 (yellow and green lines). By analyzing spectral evolution in visible domain of Fe(III)/(**7**) system at different pH, we observed a behavior comparable to other Fe(III)/ hydroxypyrones systems. [40], [41], [42] By analogy, therefore it is reasonable to assume that increasing pH: i) increase the number of chelating molecules coordinating the metal and that ii) ligand (**7**) coordinates iron(III) *via* the phenol and keto oxygen atoms of hydroxypyrone surely at acid pH. However, this does not exclude that

malonate moiety play a role in metal coordination as Infrared and Raman spectroscopy measurement highlight (sez. 3.3.2).

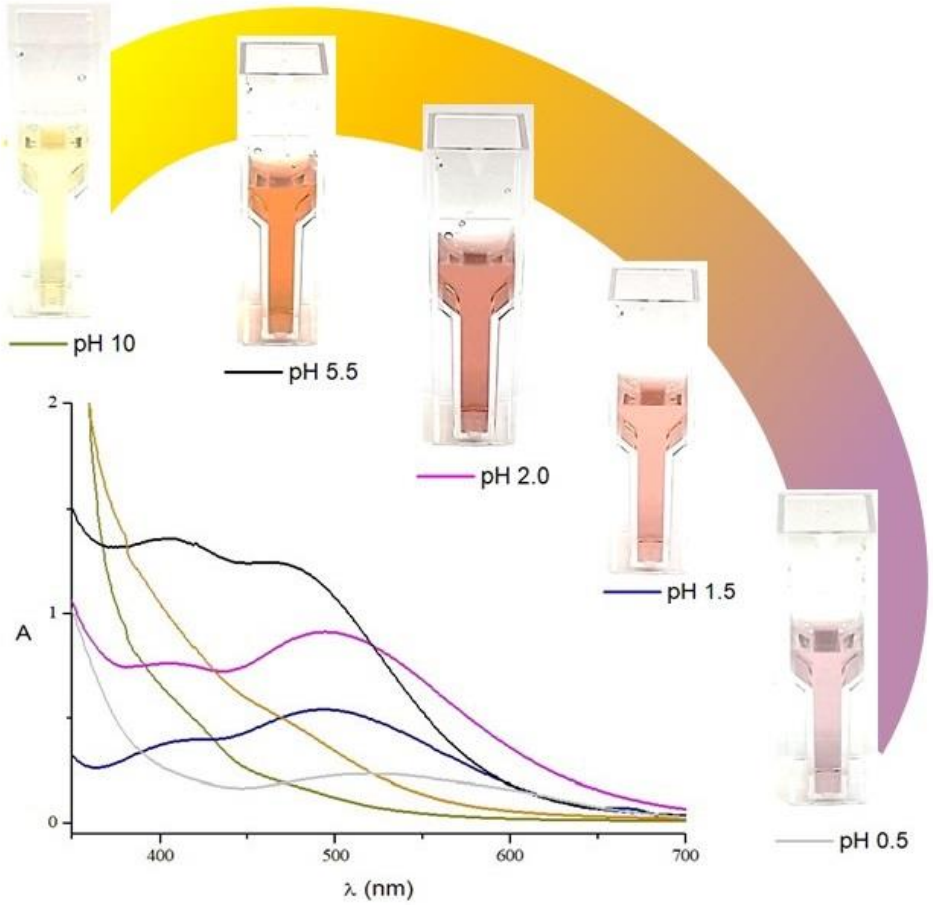

Fig. 4. Spectra collected in a pH range 0.5-10 of solution containing [Fe^{3+}] =0.7 x 10^{-3} M and [**7**] = 2.2 x 10^{-3} M ; T = 298 K. Cell path: 1 cm.

3.3.2 Infrared and Raman spectroscopy

Carboxylate groups can coordinate metal in different ways: (a) ionic, (b) unidentate chelating or (c) bidentate chelating coordination and (d) bidentate bridging coordination (Scheme 4).

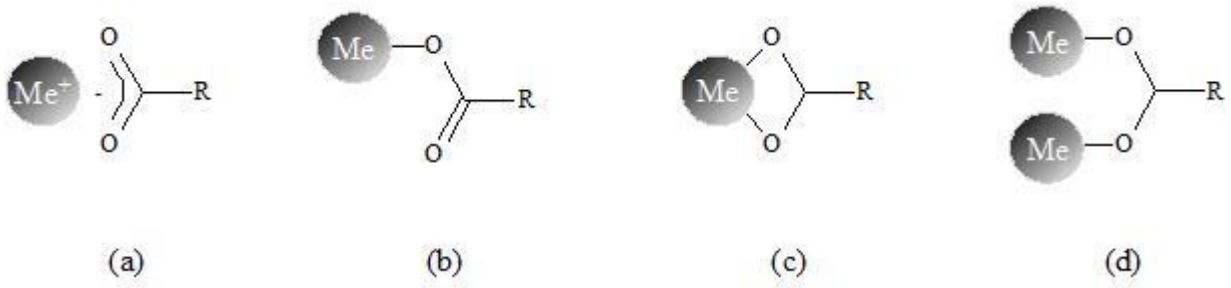

Scheme 4. Structure of metal carboxylates according to the type of metal-ligand interaction (Me = metal).

Among the most sensible vibration bands affected by the coordination are $\nu_{as}(COO-)$ and $\nu_{s}(COO-)$ bands. In the case of Fe(III) complexes with substituted malonic acid, these bands are attended in the regions 1690-1590 and 1430-1400 cm^{-1}, respectively [43]. The separation of the bands $\Delta\nu = \nu_{as}(COO-)-\nu_{s}(COO-)$ is highly sensitive to the nature of the solvent / ligand / metal ion, and the magnitude of separation should be compared with that of simple ionic carboxylates, usually taken as the sodium salt.

As suggested by Nakamoto [44] about metal-carboxylate, if $\Delta\nu_{complex} \ll \Delta\nu_{Na}$ then a bidentate chelating coordination is attended, if $\Delta\nu_{complex} \gg \Delta\nu_{Na}$ is indication of a unidentate coordination.

FTIR spectra of (**3**) showed the bands ascribed to the antisymmetric and symmetric stretching vibration of carboxylate ligands at 1570 and 1434 cm^{-1} respectively. The magnitude of

separation, $\Delta\nu$ = 136 cm^{-1}, increase to 167 cm^{-1} with iron(III) coordination (Fig. 5). Similarly, Fe(III) coordination to (**7**) caused an apparent increase of $\Delta\nu$ (Fig. S16).

By analogy with other metal-acetates [45] and metal-carboxylates [46] stretching frequency, we suppose a unidentate nature of carboxylate moiety.

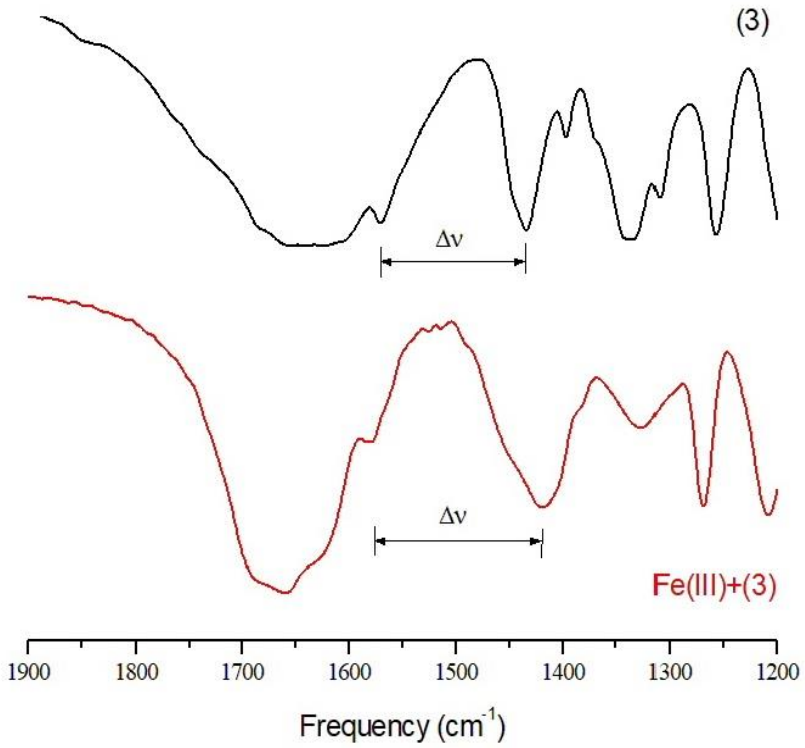

Fig. 5. Spectrum of (**3**) (black line) and Fe(III)/(**3**) (red line) in KBr pellet. Sample was obtained from acid solution

Raman spectra of maltol, (**3**) and (**7**) and related ferric solution at pH 4.5 and 7.2 were also recorded (Fig. S16-S19). According to ionic nature of (**3**), Raman bands at 1560 and 1436 cm^{-1} should be assigned to carboxylates asymmetric and symmetric stretching. These bands were not present in Raman spectra of maltol while collapsed into a single band at 1510 cm^{-1} in the case of

(**7**), as consequence of metal coordination of carboxylic group a new band at 1480 cm^{-1} appeared (Fig. S20). Moreover, both at pH 4.4 and 7.2, Raman spectra of Fe(III)/(**7**) and Fe(III)/(**Malt**) showed a couple of bands at 1565 and 610 (broad) cm^{-1} and 1615 and 615 (broad) cm^{-1} respectively, probably associated to pyrone/Fe(III) chelate mode.

To conclude, both Infrared and Raman spectral studies indicate a monodentate nature of carboxylate group where malonate moiety acts as bidentate chelator. Furthermore, Raman as well as UV-Vis spectra, suggest that (**7**) and maltol may coordinate iron(III) ion through oxygen atoms of 3-hydroxy and carbonilic groups of γ-pyrone (Scheme 5).

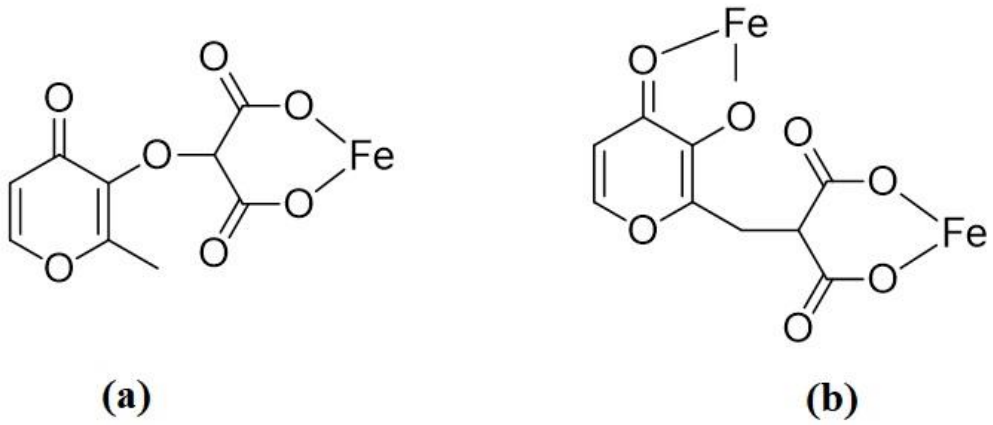

Scheme 5. Proposed metal binding sites of (**3**) and (**7**).

3.3.3 Computational verification of the chelation modes

We attempted to verify the chelation modes by crystallographic means but were not able to obtain any viable result. Therefore, we decided to perform a series of *in silico* tests, and thus verify the possible chelating modes. First, we tested two complexes between compound (**3**), Fe(III); Model 1 featured 1 molecule of compound (**3**) and 4 molecules of water, while Model 2 comprised 2 molecules of compound (**3**) and 2 molecules of water. As shown in Figure 6, topmost

panels, the optimized structure of Model 1 shows the expected chelating modes of (**3**). The two carboxylic moieties are perpendicular to each other and chelate the iron ion. Moreover, one oxygen atom of the two carboxylic group not involved in legating Fe(III) is positioned so as to form a hydrogen bond with one water molecule. Model 2 optimized structure shows a possible arrangement of 2 molecules of compound (**3**) chelating the same Fe(III) ion.

Figure 6, middle-top panels, show the optimized structures of compound (**7**) chelating iron, together with 4 explicit water molecules. Model 3 chelates through its carboxylic moieties, while Model 4 chelates through the 3-hydroxy oxygen atoms. The computed energy difference between the two models is very small (0.5 kcal mol^{-1}, 1.9 J mol^{-1}), which strongly suggests that both chelating modes are equally possible, with a preference for Model 4, that is chelating with the 3-hydroxy oxygen atoms. It is notable that, while chelating with 3-hydroxy oxygen atoms, Model 4 maintains an extra hydrogen bond between one carboxylic oxygen atom and a water molecule. Model 3, instead, shows the same extra hydrogen bond with a water molecule as in Model 1.

Finally, the lowest three panels of Figure 6 show the three possible combinations of 2 molecules of compound (**7**) chelating Fe(III), along with 2 water molecules. Model 6 shows the lowest energy of the three, that is when both ligands employ their 3-hydroxy oxygen atoms. Nevertheless, the models suggest that it should be possible for compound (**7**) to form networks or chains of compounds chelating Fe(III) iron atoms. Models 5-7 also show carboxylic oxygen atoms not directly chelating the metal ion involved in hydrogen bonds with the water molecules.

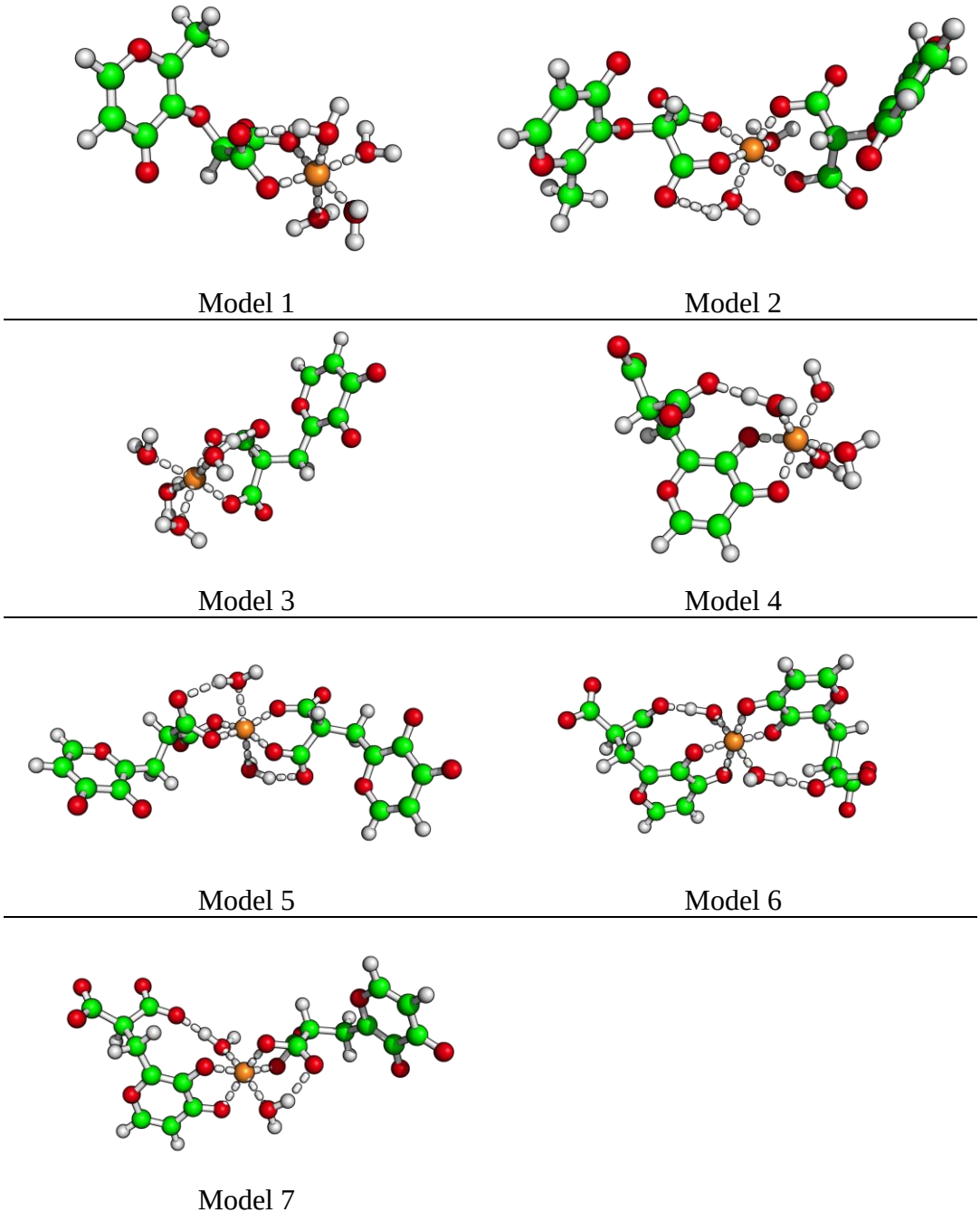

Fig. 6: Representation of the optimized structures of the different models studied by computational means. Carbon atoms are represented in green, hydrogen atoms in white, oxygen atoms in red and iron atoms in orange. Dative and hydrogen bonds are dashed.

3.3.4 Electrochemistry

Electrochemical studies were performed in aqueous solution with KNO_3 as supporting electrolyte instead of KCl, considering that the nitrate is a weaker ligand for Fe(III) than chloride and therefore avoids the competition of the anion with the chelators for the metal ion. Cyclic voltammetry experiments were performed at different metal to ligand ratio, as well as at different pHs.

In nitrogen saturated solution and pH ≤ 2, the Fe(III)/Fe(II) reduction occurred at E_{pc}= +0.25 V (not shown). Adding stoichiometric amounts of chelator to iron(III) solution, cyclic voltammograms resulted in an increased more cathodic irreversible peak while ferric-free-ion peak decrease until disappeared at molar ratio Fe/chelator 1:3 (Figure 7).

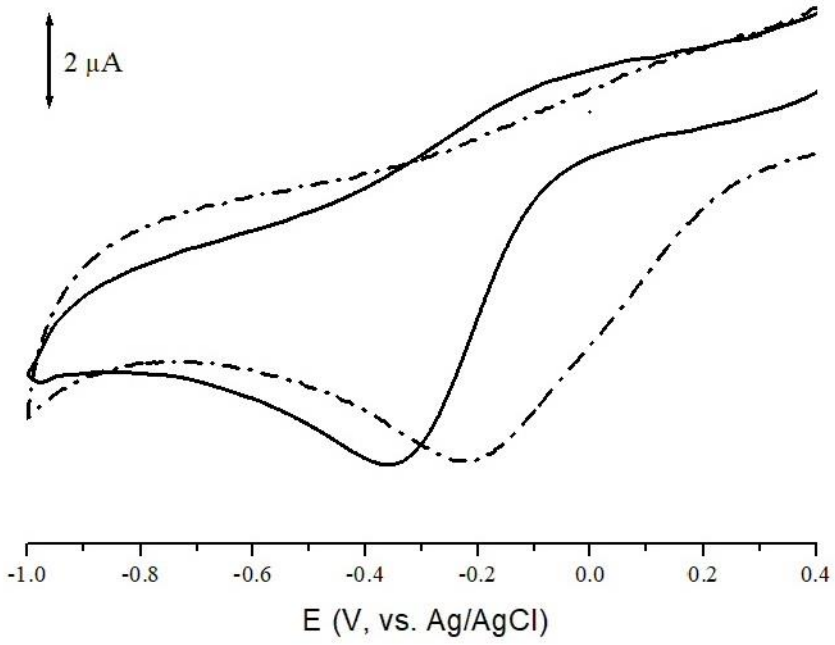

Fig. 7. Cyclic voltammograms recorded on a glassy carbon electrode of an aqueous solution of $[Fe^{3+}]$= 3.0 x 10^{-3} M and [**7**]= 9.0 x 10^{-3} M (bold line) or [**3**]= 9.0 x 10^{-3} M (dash-dotted line). Scan rate 50 mV/s.

As Table 3 shows, increasing pH peak potentials of Fe(III) complex moved to more cathodic values. This shift should be consequence of the increasing number of chelator to metal ion.

Table 3. Peak potential vs. Ag/AgCl and converted vs. NHE (in italic) measured for Fe(III) complexes at a scan rate of 50 mV/s. $[Fe^{3+}] = 2.0 \times 10^{-3}$ M.

pH	**Fe-Malt**	**Fe-(3)**	**Fe-(7)**
≤ 4	-0.23 *(-0.03)*	-0.21	-0.35 *(-0.14)*
5.5	-0.23*(-0.03)*	-0.34 *(-0.14)*	-0.35 *(-0.14)*
7.4	-0.50 *(-0.30)*[a]	-0.34[b]	-0.40 *(-0.20)*[b]

[b] Redox potential. [a] From spectroelectrochemistry data: $[Fe^{3+}] = 2.5 \times 10^{-4}$ M, [L] = 7.5×10^{-4} M

In order to determine the redox potential of ferric complexes at lower concentration and at physiologic pH, spectroelectrochemical experiments were performed. Buffered solution (pH 7.4) of Fe(III) with (**3**) or (**7**) showed an intense peak at 265 and 275 nm, respectively, and a broad band at 310-320 nm. The spectroscopic profile of solutions did not change while scanning the potential from 0 to -0.55 V in presence of both ligands. Irreversibility of reduction process observed by cyclic voltammogram, suggest that ferrous species electrogenerated were not stable at physiological pH and the release of metal was possible. For this reason, the stability of reduced specie was tested applying a constant potential (E_w = -0.70 V) for 10 minutes. As expected, in the longer time of electrolysis, some precipitation occurred. To confirm this hypothesis, the experiment was repeated in presence of 1,10 phenanthroline (phen), a Fe(II) selective ligand. In this conditions, precipitation did not occurred and the characteristic UV-vis band of iron(II)-phen complex appeared (not shown).

Spectroelectrochemical experiment were also carried out on Fe(III)/(**7**) (1:5) in acetate buffer solution. The cycle voltammogram shows an irreversible reduction with peak potential Ep = -0.35 V. Applying variable potential between 0 and -0.60 V the color of solution changes from violet to yellow. On the left side of Figure 8 ware reported the spectra recorded during reduction of Fe(III)/(**7**). As arrows indicate, the consequence of addition of electrons was that the two lower energy absorption bands tend to disappear. The back scan of potential and the consequent oxidation of Fe(II)→Fe(III), involves restoring of initial violet solution.

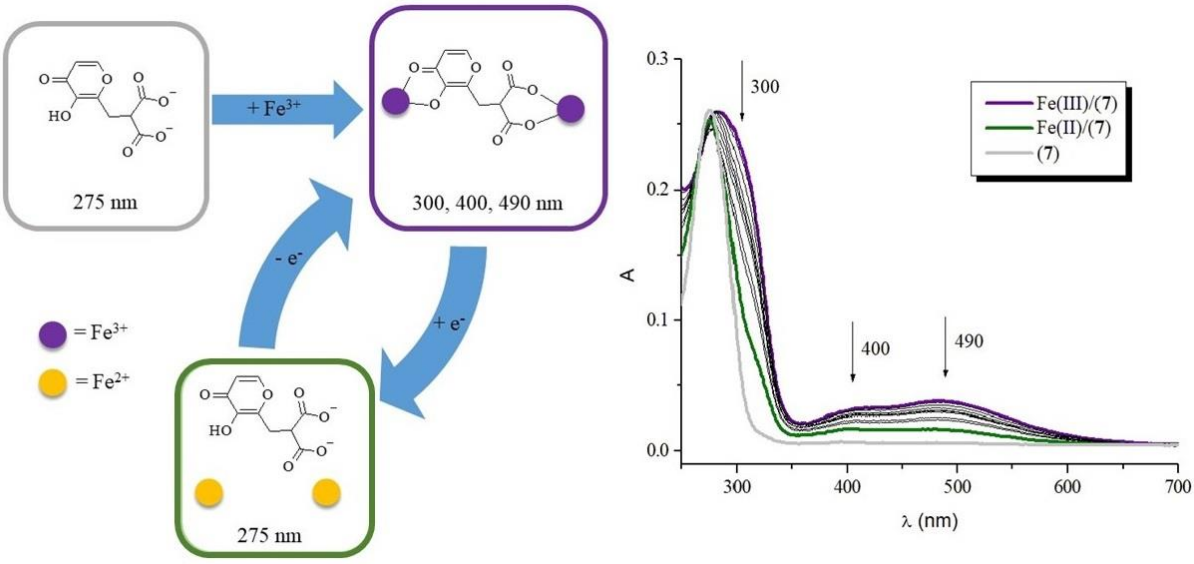

Fig. 8. Spectral UV-Vis changes recorded during progressive reduction of a solution containing $Fe(NO_3)_3$ (0.2 x 10^{-3} M) and (**7**) (1.0 x 10^{-3} M) in acetate buffer solution and corresponding metal binding sites map.

The interpretation of spectroelectrochemical data is schematized on the right side of Figure 8 where is illustrated the probable coordination sites of iron as function of its oxidation state. The

scheme was divided in squares, each of them reports a proposed reaction stage and the relative wavelength of the main bands observed in UV-vis spectrum too.

As starting point, in the grey box is reported the scheme of ligand and the wavelength of the main band (275 nm). This band is assigned to the $\pi \rightarrow \pi^*$ transition of to the hydroxypyrone chromophore. The Fe(III) addition to ligand solution (violet box), implies the change of color from yellow to violet. The corresponding UV-Vis spectrum showed three main bands at 300, 400 and 490 nm. The bathocromic shift of the ultraviolet band was interpreted as an active involvement of hydroxypyrone core in metal coordination. The appearance of two long-wavelength absorption bands, due to $d \rightarrow d^*$ transitions, provide evidence of formation of iron derivative(s) of (**7**). Similar spectra are reported for other ferric hydroxypyrone complexes. [40],[41],[42],[47]

Finally, the green box of Figure 8 shows the restored free ligand and the release of iron, after electrochemical reduction of Fe(III)-complex(es). The UV-vis spectrum, corresponding to this stage of the process, presents again the strong absorption band at 275 nm.

As Fig. 8 outlines, as consequences of metal coordination two relevant points emerge: i) deprotonation of OH group of hydroxypyrone results in the appearance of a broad band at 300 nm and ii) appearance of two visible absorptions at 400 and 490 nm. Electrochemical reduction of complex involves release of Fe(II) and re-protonation of OH group with restoring of original UV-vis spectra.

Spectroelectrochemical experiment at pH 4.5 on Fe(III)/(**3**) solution does not add information on iron binding mode of (**3**) either on ferric complex behavior during reduction (Fig. S20)

In conclusion, electrochemical data highlight the existence of ferric complexes of (**3**) and (**7**) that undergo to an irreversible reduction process with a pH-dependent cathodic peak. The

irreversibility of process was likely due to ligand dissociation event, which occurred in the reduced form of the complexes. Ion Fe(II) is a softer Lewis acid and its interaction with oxygen atom is not thermodynamically favored as that with a hard Fe(III) ion. Therefore, this great loss in thermodynamic stability facilitated the release of iron from stable complexes and an irreversible process occurred. It is discussed that iron-maltol complex exerts its function of reservoir of soluble iron through reductive mechanism. After reduction of ferric complex in the gut lumen, dissociation of metal and ligand takes place and the Fe(II) ion is readily available for uptake at the intestinal cell surface [48]. Consequently, reduction of a Fe(III)-complex followed by ligand exchange appears to be a viable mechanism for iron release and incorporation into a cell. Looking at Table 2, this redox hypothesis seems reasonable because ferric complexes could be reducible by biologic agent such as NADH or NADP, which has a redox potential of -0.32 V (vs. NHE, pH 7.0) [49].

3.3.5 Electron paramagnetic resonance

To clarify the geometry and the electronic structure of iron complexes, electron paramagnetic resonance spectra at different pH were recorded.

X-band (9GHz) EPR spectra were recorded at 130K and they are characterized by Fe(III) (S=5/2) signal contributions. For paramagnetic species with more than one unpaired electron such as Fe(III), the interaction between the paramagnetic electrons and the ligand field leads to a separation in the energies of the spin states (MS=±1/2, ±3/2, ±5/2) even in the absence of an external magnetic field. This generates the zero-filed splitting effect (ZFS). When ZFS=0 no splitting is present and D=0, therefore a single isotropic line is present centered around g=2.0. If the splitting is small, five lines with a g=2 are present. When the zero-field splitting is large an axial geometry is visible with two g values: $g_{\parallel}$=2 and $g_{\perp}$=6. [50],[51],[52],[53]. In

all the samples analyzed a pure axial contribution is not present as the intense peak at g=6 typical of such geometry is not visible. Deviations from this value (for example g~5) shows a high spin contribution slightly distorted from axial geometry. With symmetries lower than axial a second parameter E is used to describe the rhombic distortion. When E/D=1/3 a diagnostic signal of high spin iron in strongly rhombic site centered around g=4.3 is evident due to the transition of Ms=±3/2 and two very low transitions around g=9 and g=0.6-0.9 may be also visible. In all spectra the 4.3 transition is evident suggesting a strong rhombic distortion and, in some cases, also a low contribution at g around 8 is present.

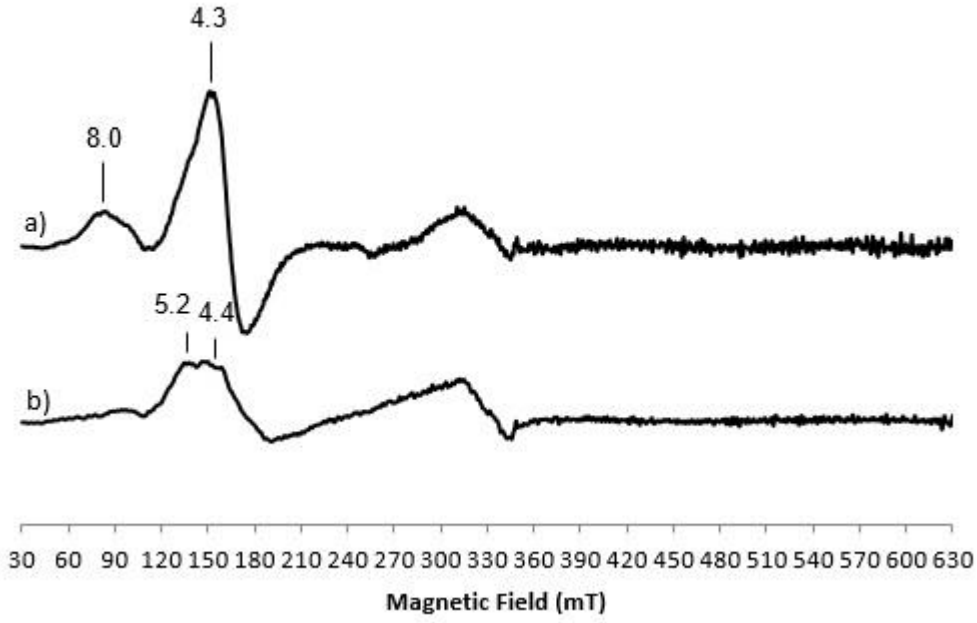

Fig. 9. X-band (9GHz) EPR spectra of ferric solution of a) (**3**), b) (**7**) at pH ~ 3 and 130K. Experimental conditions: ν=9.67GHz, 1mT modulation amplitude and 16mW microwave power.

X-band EPR spectra of aerobic ferric solution of (**3**) and (**7**) at acid pH were recorded at 130K. In Figure 9a) it is evident the predominance of the rhombic contribution with g=4.3, whereas

in Fig. 9b) there is the contemporary presence of the rhombic and distorted axial species. All the contributions for Fe(III) characterized in this paper are also present in iron-catecholate complexes reported in [54].

X-band EPR spectra of ferric solution of (**3**) and (**7**) at basic pH (pH ~ 8) were also recorded. In both spectra there is the contemporary presence of the rhombic and distorted axial species even though in Fig. 10b) the orthorhombic contribution with g = 4.3 is more evident.

The g ≈ 4.3 hs-Fe^{3+} signal became progressively more intense increasing pH likely consequence of the progression from mono- to bis- (or tris?) chelate complexes.

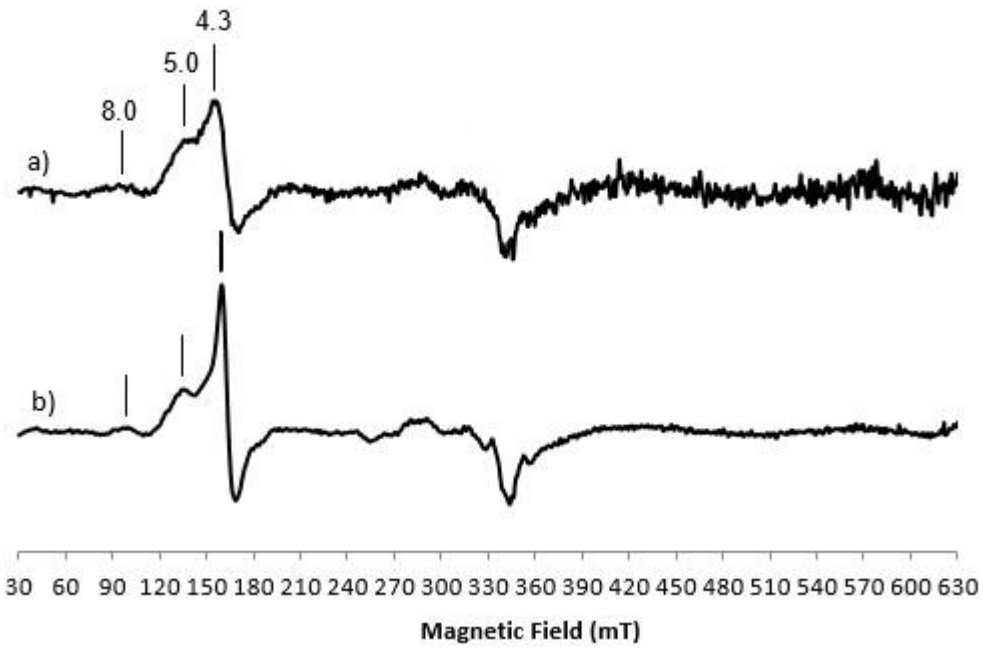

Fig. 10. X-band (9GHz) EPR spectra of ferric solution of a) (**3**), b) (**7**) at pH ~ 8 and 130K. Experimental conditions: ν=9.67GHz, 1mT modulation amplitude and 16mW microwave power.

3.3.6 Antioxidant and antiradicalic activity

Oxidative stress is one of the potential biochemical mechanisms involved in the pathogenesis of ID. [55] Some exogenous factors such as drugs and transition metals, leading to oxygen and nitrogen reactive species generation (ROS and RNS, respectively). Alteration of the balance between ROS and RNS production and the cell capacity to rapidly detoxify reactive intermediates lead to oxidative stress. The antioxidant defense system comprises both enzymatic and nonenzymatic mechanisms: in general, antioxidants help the body to defend against the effects of ROS/RNS removing free radicals from the system and inhibiting oxidation by being oxidized themselves. [56] In addition, some molecules considered as antioxidants (maltol, vitamin A and C) show to increase iron absorption. [57]

In this context as preliminary tests, we evaluated the possible antioxidant effects of ligands in different *in vitro* antioxidant assays using the deoxyribose degradation method and 1,1-diphenyl-2-picryl-hydrazyl free radical (DPPH) scavenging method.

Hydroxyl radicals, formed by a combination of ascorbic acid, H_2O_2 and Fe(III)–EDTA complex, can easily interact with deoxyribose giving rise to products which yield a pink chromogen after heating with thiobarbituric acid. When compounds with hydroxyl radical "scavengers" properties are present in the solution mixture, they compete with deoxyribose for the hydroxyl radicals, thus lowering the formation of the colored chromogen. Results showed that this was the case for (**3**) and (**7**), which inhibited the formation of the pink chromogen in a concentration-dependent fashion, with IC_{50} value of (mean ± e.s.m, $x10^{-3}$ M) 5.58±0.76 and 2.14±0.46, respectively. Maltol, used as reference compound, had IC_{50} value of 2.44±0.1, suggesting that the potency of (**7**) and (**3**) was comparable to maltol itself.

The DPPH method is based on the reduction of DPPH· in alcoholic solution in the presence of a hydrogen-donating molecules and it is the most frequently used one for *in vitro* antioxidant activity. The scavenging ability was affected by the structural features of the antioxidant molecule,

for example by the length of conjugated double bonds or stability of radical. Besides, the trend of antioxidant activity, ranging from the strongest to the weakest, was: (**7**) > (**3**) > Malt (IC_{50} 3.15 ± 0.40; 4.96 ± 0.29; > 7 mM respectively). This can be explained according to the differences in their chemical structures. The compounds in this study belong to the pyranone ring containing compounds but differ for substituents. After reaction with DPPH, (**7**)$^{\cdot}$ and (**3**)$^{\cdot}$ were probably stabilized by resonance through carboxylic oxygen and this increased their antioxidant efficiency for DPPH in comparison to maltol.

4. Conclusion

The aim of this work was to synthetize new water soluble iron chelators able to solubilize Fe(III) in physiologic conditions. Their iron coordination ability was assessed in solution by UV-Vis IR, Raman, EPR spectroscopy and electrochemistry. Ligand (**3**) adopts mainly bidentate coordination mode through oxygen atoms of malonate moiety while ligand (**7**) has two equally possible metal binding sites. As electrochemical data highlight, at pH 7.2 the ferric complexes of (**3**) and (**7**) were more easily reduced than the $[Fe(Mal)_3]$ while irreversibility of the process should promote the reduction mechanism postulated for oral iron drugs. Moreover, introduction of acid function on γ-pyrone does not appear to alter its antiradicalic and antioxidant properties.

In conclusion, the properties highlighted in the present study strongly suggest that compounds (**3**) and (**7**) can be the starting point to prepare novel and safe pyrone-based compound for Fe(III) supplement in ID disorders.

Acknowledgments

Grateful thanks are due to Prof. Marco Ferrali (University of Siena, retired) for his constructive suggestions. M. C. thanks the Consorzio Interuniversitario di Ricerca in Chimica dei Metalli nei Sistemi Biologici (CIRCMSB) for stimulating discussions. T.R. and K.Z. acknowledge the financial support from the Danish National Research Foundation (DNRF122) and Villum Fonden (Grant No. 9301) for Intelligent Drug delivery and sensing Using microcontainers and Nanomechanics (IDUN). S.F., M.C.B., L.D.V. and M.C. acknowledge a MIUR (Ministero dell'Istruzione, dell'Università e della Ricerca) grant "Dipartimento di Eccellenza 2018 - 2022".

Conflicts of interest

The authors declare no conflict of interest.

References

[1] H. Ludwig, E. Müldür, G. Endler, W. Hübl, Prevalence of iron deficiency across different tumors and its association with poor performance status, disease status and anemia, Annals of Oncology. 24 (2013) 1886–1892. https://doi.org/10.1093/annonc/mdt118.

[2] C. Gargallo-Puyuelo, E. Alfambra, J. García-Erce, F. Gomollon, Iron Treatment May Be Difficult in Inflammatory Diseases: Inflammatory Bowel Disease as a Paradigm, Nutrients. 10 (2018) 1959. https://doi.org/10.3390/nu10121959.

[3] P. Santiago, Ferrous versus Ferric Oral Iron Formulations for the Treatment of Iron Deficiency: A Clinical Overview, The Scientific World Journal. 2012 (2012) 1–5. https://doi.org/10.1100/2012/846824.

[4] T.S. Koskenkorva-Frank, G. Weiss, W.H. Koppenol, S. Burckhardt, The complex interplay of iron metabolism, reactive oxygen species, and reactive nitrogen species: Insights into the potential of various iron therapies to induce oxidative and nitrosative stress, Free Radical Biology and Medicine. 65 (2013) 1174–1194. https://doi.org/10.1016/j.freeradbiomed.2013.09.001.

[5] A. Di Castelnuovo, R. di Giuseppe, L. Iacoviello, G. de Gaetano, Consumption of cocoa, tea and coffee and risk of cardiovascular disease, European Journal of Internal Medicine. 23 (2012) 15–25. https://doi.org/10.1016/j.ejim.2011.07.014.

[6] Z. Tolkien, L. Stecher, A.P. Mander, D.I.A. Pereira, J.J. Powell, Ferrous Sulfate Supplementation Causes Significant Gastrointestinal Side-Effects in Adults: A Systematic Review and Meta-Analysis, PLOS ONE. 10 (2015) e0117383. https://doi.org/10.1371/journal.pone.0117383.

[7] M.W. Whitehead, R.P. Thompson, J.J. Powell, Regulation of metal absorption in the gastrointestinal tract., Gut. 39 (1996) 625–628. https://doi.org/10.1136/gut.39.5.625.

[8] R. Bentley, From miso, saké and shoyu to cosmetics: a century of science for kojic acid, Natural Product Reports. 23 (2006) 1046. https://doi.org/10.1039/b603758p.

[9] N. Yang, C. Liu, X. Liu, T.K. Degn, M. Munchow, I. Fisk, Determination of volatile marker compounds of common coffee roast defects, Food Chemistry. 211 (2016) 206–214. https://doi.org/10.1016/j.foodchem.2016.04.124.

[10] G.A. Burdock, M.G. Soni, I.G. Carabin, Evaluation of Health Aspects of Kojic Acid in Food, Regulatory Toxicology and Pharmacology. 33 (2001) 80–101. https://doi.org/10.1006/rtph.2000.1442.

[11] K.H. Thompson, C.A. Barta, C. Orvig, Metal complexes of maltol and close analogues in medicinal inorganic chemistry, Chemical Society Reviews. 35 (2006) 545. https://doi.org/10.1039/b416256k.

[12] C.V. Credille, B.L. Dick, C.N. Morrison, R.W. Stokes, R.N. Adamek, N.C. Wu, I.A. Wilson, S.M. Cohen, Structure–Activity Relationships in Metal-Binding Pharmacophores for Influenza Endonuclease, Journal of Medicinal Chemistry. 61 (2018) 10206–10217. https://doi.org/10.1021/acs.jmedchem.8b01363.

[13] M. Corsini, S. Fusi, Synthesis, characterization of 3-hydroxy-2-(5-hydroxypentyl)-4H-pyran-4-one and related iron(III) complexes, Russian Journal of Inorganic Chemistry, 64, (2019),1836–1840.https://doi.org/10.1134/S003602361914002X

[14] Z.D. Liu, H.H. Khodr, D.Y. Liu, S.L. Lu, R.C. Hider, Synthesis, Physicochemical Characterization, and Biological Evaluation of 2-(1‘-Hydroxyalkyl)-3-hydroxypyridin-4-ones: Novel Iron Chelators with Enhanced pFe $^{3+}$ Values †, Journal of Medicinal Chemistry. 42 (1999) 4814–4823. https://doi.org/10.1021/jm991080o.

[15] Shield Therapeutics announces submission of a New Drug Application (NDA) for Feraccru® for the treatment of iron deficiency with the US Food and Drug Administration (FDA) [news release]. Shield Therapeutics plc., (2018). https://www.shieldtherapeutics.com/rns_news/submission-of-an-nda-for-feraccru-with-the-fda/ (accessed February 18, 2020).

[16] R.S.J. Harvey, D.M. Reffitt, L.A. Doig, J. Meenan, R.D. Ellis, R.P.H. Thompson, J.J. Powell, Ferric trimaltol corrects iron deficiency anaemia in patients intolerant of iron, Alimentary Pharmacology and Therapeutics. 12 (1998) 845–848. https://doi.org/10.1046/j.1365-2036.1998.00380.x.

[17] Feraccru | European Medicines Agency, https://www.ema.europa.eu/medicines/human/EPAR/feraccru.

[18] C. Gasche, T. Ahmad, Z. Tulassay, D.C. Baumgart, B. Bokemeyer, C. Büning, S. Howaldt, A. Stallmach, Ferric Maltol Is Effective in Correcting Iron Deficiency Anemia in Patients with Inflammatory Bowel Disease: Results from a Phase-3 Clinical Trial Program, Inflammatory Bowel Diseases. 21 (2015) 579–588. https://doi.org/10.1097/MIB.0000000000000314.

[19] P.E. Pergola, S. Fishbane, T. Ganz, Novel Oral Iron Therapies for Iron Deficiency Anemia in Chronic Kidney Disease, Advances in Chronic Kidney Disease. 26 (2019) 272–291. https://doi.org/10.1053/j.ackd.2019.05.002.

[20] A. Böcker, P.R. Bonneau, O. Hucke, A. Jakalian, P.J. Edwards, Development of Specific "Drug-Like Property" Rules for Carboxylate-Containing Oral Drug Candidates, ChemMedChem. 5 (2010) 2102–2113. https://doi.org/10.1002/cmdc.201000355.

[21] M. Ehrlich, T. Carell, Total Syntheses and Biological Evaluation of 3- *O* -Methylfunicone and Its Derivatives Prepared by TMPZnCl·LiCl-Mediated Halogenation and Carbonylative Stille Cross-Coupling: Total Synthesis and Biological Evaluation of 3- *O* -Methylfunicones, European Journal of Organic Chemistry. 2013 (2013) 77–83. https://doi.org/10.1002/ejoc.201201256.

[22] B. Halliwell, J.M.C. Gutteridge, O.I. Aruoma, The deoxyribose method: A simple "test-tube" assay for determination of rate constants for reactions of hydroxyl radicals, Analytical Biochemistry. 165 (1987) 215–219. https://doi.org/10.1016/0003-2697(87)90222-3.

[23] S. Chaves, S. Canário, M.P. Carrasco, L. Mira, M.A. Santos, Hydroxy(thio)pyrone and hydroxy(thio)pyridinone iron chelators: Physico-chemical properties and antioxidant activity, Journal of Inorganic Biochemistry. 114 (2012) 38–46. https://doi.org/10.1016/j.jinorgbio.2012.04.019.

[24] A. Neri, M. Frosini, M. Valoti, M.G. Cacace, E. Teodori, G. Sgaragli, N, N-Bis(cyclohexanol)amine aryl esters inhibit P-glycoprotein as transport substrates, Biochemical Pharmacology. 82 (2011) 1822–1831. https://doi.org/10.1016/j.bcp.2011.08.025.

[25] M. Biagi, G. Collodel, M. Corsini, N.A. Pascarelli, E. Moretti, Protective effect of Propolfenol ® on induced oxidative stress in human spermatozoa, Andrologia. 50 (2018) e12807. https://doi.org/10.1111/and.12807.

[26] W. Kohn, L.J. Sham, Self-Consistent Equations Including Exchange and Correlation Effects, Physical Review. 140 (1965) A1133–A1138. https://doi.org/10.1103/PhysRev.140.A1133.

[27] V.A. Rassolov, J.A. Pople, M.A. Ratner, T.L. Windus, 6-31G * basis set for atoms K through Zn, The Journal of Chemical Physics. 109 (1998) 1223–1229. https://doi.org/10.1063/1.476673.

[28] A.D. Becke, Density-functional thermochemistry. III. The role of exact exchange, The Journal of Chemical Physics. 98 (1993) 5648–5652. https://doi.org/10.1063/1.464913.

[29] J. Tomasi, B. Mennucci, R. Cammi, Quantum Mechanical Continuum Solvation Models, Chemical Reviews. 105 (2005) 2999–3094. https://doi.org/10.1021/cr9904009.

[30] I. Fdez. Galván, M. Vacher, A. Alavi, C. Angeli, F. Aquilante, J. Autschbach, J.J. Bao, S.I. Bokarev, N.A. Bogdanov, R.K. Carlson, L.F. Chibotaru, J. Creutzberg, N. Dattani, M.G. Delcey, S.S. Dong,

A. Dreuw, L. Freitag, L.M. Frutos, L. Gagliardi, F. Gendron, A. Giussani, L. González, G. Grell, M. Guo, C.E. Hoyer, M. Johansson, S. Keller, S. Knecht, G. Kovačević, E. Källman, G. Li Manni, M. Lundberg, Y. Ma, S. Mai, J.P. Malhado, P.Å. Malmqvist, P. Marquetand, S.A. Mewes, J. Norell, M. Olivucci, M. Oppel, Q.M. Phung, K. Pierloot, F. Plasser, M. Reiher, A.M. Sand, I. Schapiro, P. Sharma, C.J. Stein, L.K. Sørensen, D.G. Truhlar, M. Ugandi, L. Ungur, A. Valentini, S. Vancoillie, V. Veryazov, O. Weser, T.A. Wesołowski, P.-O. Widmark, S. Wouters, A. Zech, J.P. Zobel, R. Lindh, OpenMolcas: From Source Code to Insight, Journal of Chemical Theory and Computation. 15 (2019) 5925–5964. https://doi.org/10.1021/acs.jctc.9b00532.

[31] Y. Ni, G. Zhang, S. Kokot, Simultaneous spectrophotometric determination of maltol, ethyl maltol, vanillin and ethyl vanillin in foods by multivariate calibration and artificial neural networks. Food Chemistry, 89, Issue 3, (2005), 465-473, https://doi.org/10.1016/j.foodchem.2004.05.037.

[32] E5: Acid Dissociation Constants of Organics, Chemistry LibreTexts. (2013). https://chem.libretexts.org/Ancillary_Materials/Reference/Reference_Tables/Equilibrium_Constants/E5%3A_Acid_Dissociation_Constants_of_Organics (accessed January 7, 2019).

[33] ChemAxon - Software Solutions and Services for Chemistry & Biology, (n.d.). https://chemaxon.com/products/jchem-for-office (accessed October 26, 2018).

[34] L. Alderighi, P. Gans, A. Ienco, D. Peters, A. Sabatini, A. Vacca, Hyperquad simulation and speciation (HySS): a utility program for the investigation of equilibria involving soluble and partially soluble species, Coordination Chemistry Reviews. 184 (1999) 311–318. https://doi.org/10.1016/S0010-8545(98)00260-4.

[35] C.A. Lipinski, F. Lombardo, B.W. Dominy, P.J. Feeney, Experimental and computational approaches to estimate solubility and permeability in drug discovery and development settings, Advanced Drug Delivery Reviews. 23 (1997) 3–25. https://doi.org/10.1016/S0169-409X(96)00423-1.

[36] V. Salvadó, X. Ribas, V. Zelano, G. Ostacoli, M. Valiente, The chemistry of iron in biosystems—III. Complex formation between FeIII and malonic acid in aqueous solutions, Polyhedron. 8, (1989), 813-818. https://doi.org/10.1016/S0277-5387(00)83851-6.

[37] Z. Wang, C. Xi, H. Ji, W. Ma, C. Chen, C, J. Zhao, Photochemical cycling of iron mediated by dicarboxylates: special effect of malonate, Environmental Science & Technology, 44, (2010), pp. 263-268. http://doi.org/10.1021/es901956x

[38] R. H. Holm, F. A. Cotton, Spectral Investigations of Metal Complexes of β-Diketones. I. Nuclear Magnetic Resonance and Ultraviolet Spectra of Acetylacetonates, J. Am. Chem. Soc. 80, (1958), 5658–5663. https://doi.org/10.1021/ja01554a020.

[39] B. A. Dekkiche, N. Seraghni, N. Debbache, I. Ghoul, T. Sehili, Effect of Natural and Artificial Light on Fe(III) Organic Complexes Photolysis: Case of Fe (III)-Malonate and Fe(III)-Malate, International Journal of Chemical Reactor Engineering. 17 (2018) https://doi.org/10.1515/ijcre-2018-0106.

[40] I.A. Antipova, S.A. Mukha, S.A. Medvedeva, Determination of composition and instability constants of maltol complexes with iron(iii) ions, Russian Chemical Bulletin. 53 (2004) 780–784. https://doi.org/10.1023/B:RUCB.0000037841.67079.2b.

[41] V.M. Nurchi, G. Crisponi, J.I. Lachowicz, M. de G. Jaraquemada-Pelaez, C. Bretti, M. Peana, S. Medici, M.A. Zoroddu, Equilibrium studies of new bis-hydroxypyrone derivatives with Fe3+, Al3+, Cu2+ and Zn2+, Journal of Inorganic Biochemistry. 189 (2018) 103–114. https://doi.org/10.1016/j.jinorgbio.2018.09.013;

[42] V. M. Nurchi, G. Crisponi, J. I. Lachowicz, S. Murgia, T. Pivetta, M. Remelli, A. Rescigno, J.Niclós-Gutíerrez, J. M. González-Pérez, A. Domínguez-Martín, A. Castiñeiras, Z. Szewczuk, Iron(III) and aluminum(III) complexes with hydroxypyrone ligands aimed to design kojic acid derivatives with new perspectives, Journal of Inorganic Biochemistry, (104), 2010, 560-569.https://doi.org/10.1016/j.jinorgbio.2010.01.007.

[43] R.B. Lanjewar, A. N. Garg, Mossbauer, infrared and thermal decomposition studies of Iron(III) complexes with substituted malonic acids, Indian Journal of Chemistry. 30A (1991), 166–171. http://nopr.niscair.res.in/handle/123456789/41793.

[44] K. Nakamoto, Infrared and Raman spectra of Inorganic and Coordination Compounds, 3rd ed., Wiley Interscience, USA, 1978.

[45] C.T. Dziobkowski, J.T. Wrobleski, D.B. Brown, Magnetic properties and Moessbauer spectra of several iron (III)-dicarboxylic acid complexes, Inorganic Chemistry. 20 (1981) 671–678. https://doi.org/10.1021/ic50217a007.

[46] S.K. Papageorgiou, E.P. Kouvelos, E.P. Favvas, A.A. Sapalidis, G.E. Romanos, F.K. Katsaros, Metal–carboxylate interactions in metal–alginate complexes studied with FTIR spectroscopy, Carbohydrate Research. 345 (2010) 469–473. https://doi.org/10.1016/j.carres.2009.12.010.

[47] M. Ferrali, D. Donati, S. Bambagioni, M. Fontani, G. Giorgi, A. Pietrangelo, 3-Hydroxy-(4 H)-benzopyran-4-ones as potential iron chelating agents in vivo, Bioorganic & Medicinal Chemistry. 9 (2001) 3041–3047. https://doi.org/10.1016/S0968-0896(01)00207-3.

[48] M. A. Barrand, B. A. Callingham, P. Dobbin, R. C. Hider, Dissociation of a Ferric Maltol Complex and Its Subsequent Metabolism During Absorption Across the Small Intestine of the Rat, British Journal of Pharmacology. 102, (1991), 723-729. DOI: 10.1111/j.1476-5381.1991.tb12240.x

[49] H. Boukhalfa, A. L. Crumbliss, Chemical aspects of siderophore mediated iron transport, Biometals. 15, (2002), 325–339. https://doi.org/10.1023/A:1020218608266.

[50] G. Palmer, The electron paramagnetic resonance of metalloproteins, Biochemical Society Transactions. 13 (1985) 548–560. https://doi.org/10.1042/bst0130548.

[51] K. Zaremba, W. Lasocha, A. Adamski, J. Stanek, A. Pattek-Janczyk, Crystal structure and magnetic properties of tris(2-hydroxymethyl-4-oxo-4H-pyran- 5-olato-κ ^{2} O ^{5} ,O ^{4})iron(III), Journal of Coordination Chemistry. 60 (2007) 1537–1546. https://doi.org/10.1080/00958970601084243.

[52] S. Mossin, B.L. Tran, D. Adhikari, M. Pink, F.W. Heinemann, J. Sutter, R.K. Szilagyi, K. Meyer, D.J. Mindiola, A Mononuclear Fe(III) Single Molecule Magnet with a 3/2↔5/2 Spin Crossover, Journal of the American Chemical Society. 134 (2012) 13651–13661. https://doi.org/10.1021/ja302660k.

[53] S. Hansen, W. Müller-Warmuth, J. R. Pilbrow: Transition Ion Electron Paramagnetic Resonance, Clarendon Press, Oxford 1990. Berichte Der Bunsengesellschaft Für Physikalische Chemie. 95 (1991) 1307–1307. https://doi.org/10.1002/bbpc.19910951036.

[54] J.T. Weisser, M.J. Nilges, M.J. Sever, J.J. Wilker, EPR Investigation and Spectral Simulations of Iron−Catecholate Complexes and Iron−Peptide Models of Marine Adhesive Cross-Links, Inorganic Chemistry. 45 (2006) 7736–7747. https://doi.org/10.1021/ic060685p.

[55] Imam, M.U.; Zhang, S.; Ma, J.; Wang, H.; Wang, F. Antioxidants Mediate Both Iron Homeostasis and Oxidative Stress, Nutrients. 9, (2017), 671-690. https://doi.org/10.3390/nu9070671.

[56] A. Bhattacharyya, R. Chattopadhyay, S. Mitra, S. E Crowe, Oxidative Stress: An Essential Factor in the Pathogenesis of Gastrointestinal Mucosal Diseases, Physiological Reviews. 94, (2014), 329-354. doi: 10.1152/physrev.00040.2012.

[57] C. N. Kontoghiorghe, A. Kolnagou , G. J. Kontoghiorghes: Phytochelators Intended for Clinical Use in Iron Overload, Other Diseases of Iron Imbalance and Free Radical Pathology, Molecules. 20, (2015), 20841–20872. doi:10.3390/molecules201119725.